EFFECT OF THE INNER CYLINDER ENDWALL SHAPE ON THE STABILITY OF TAYLOR-COUETTE FLOW

Ahmed Daimallah*
LEMI, Mechanical Engineering Department, Faculty of Technology,
University M'hamed Bougara of Boumerdes, ALGERIA
E-mail: a.daimallah@univ-boumerdes.dz

Mohamed Lebbi
Unité de Recherche Appliquée en Énergies Renouvelable, URAER,
Centre de Développement des Energies Renouvelables, CDER, 47133 Ghardaïa, ALGERIA

The current research aims to study how changing the endwall shape of the inner cylinder affects the appearance of Ekman cells and the onset of Taylor vortices. A two-dimensional numerical method simulates the flow between two concentric cylinders, with the inner cylinder rotating while the outer cylinder and the upper and lower endwalls remain at rest. The method of solving the Navier-Stokes equations for incompressible viscous flows is provided by the Ansys Fluent software, which is based on the finite volumes method. The geometric parameters, such as the radius ratio (η) and the height ratio (Γ), are fixed at $\eta = 0.9$ and $\Gamma = 9.85$, respectively. The working fluid is an aqueous solution ($\mu = 48$ *mPa.s*, $\rho = 1050$ *kg/m³*). The study focuses on modeling four configurations (A, B, C, and D): configuration (A) includes two flat plate endwalls, configuration (B) features a hemispherical upper endwall and a flat lower plate endwall, configuration (C) consists of a flat upper endwall and a hemispherical lower endwall, and configuration (D) comprises two hemispherical endwalls. The obtained results indicate that the appearance of Ekman cells and the transition to Taylor vortex flow are specifically delayed for configuration (D). Additionally, the friction coefficient is affected by the modification of the endwalls. Indeed, configuration (D) contributes to a reduction of the skin friction coefficient by approximately *43%* at the appearance of Ekman cells, and by *20%* near the appearance of Taylor vortices compared to configuration (A).

Key words: Taylor-Couette flow, hemispherical endwall shape, Ekman cells, Taylor vortices.

1. Introduction

The flow between two concentric rotating cylinders, called Taylor-Couette flow, is important and has many industrial applications. We report studies aimed at developing the properties of gas-lubricated bearings that can be used in precision rotating machines [1]. The presence of the endwall strongly influences the structure of the flow. Many research works focus on the effect of cylinder endwalls. The transition from Couette flow to Taylor vortex flow is accompanied by the appearance of a cell near each endwall created by the movement of the flow. Bouabdallah [2] studied experimentally various flow regimes during laminar-turbulent transition using the polarization technique. The endwall cells are generally referred to Ekman vortices [3, 4]. Several studies have focused on axial endwall, either connected to the non-rotating endwall or as an external cylinder, and their effect on flow stability. Primarily, the non-rotating endwall disrupts the axisymmetric structure near the endwall at the inception of Ekman cells, as shown in refs. [5-9]. Sobolik *et al*. [10] analyzed the influence of endwall on the appearance of Ekman cells and showed that they appear at rotation rates lower than the critical rotation rate in an infinite system for the appearance of Taylor vortices. The same authors, in 2011, investigated experimentally the shear rate at the wall and its axial and azimuthal components near the transition to the Taylor vortices [11]. Their results indicate that understanding the

---

* To whom correspondence should be addressed

components and distribution of wall shear rates helps design a device based on Taylor-Couette flow. Czarny *et al*. [12] studied the interaction between Ekman cells and Taylor vortices near the transition from Couette flow to Taylor vortex flow using a spectral numerical simulation technique. They found that endwall boundary conditions significantly change the radial velocity, influencing the bifurcation diagram near the middle of the annulus. Avila *et al*. [13] modeled numerically centrifugation, where endwalls resulted in primary instability in Taylor-Vortex flow. They proposed a benchmark solution for various approaches to endwall effects on Taylor-Couette flow stability, among industrial CFD solvers [14]. Daimallah *et al*. [15, 16] applied a visualization technique to observe the flow structure and vortex shape as functions of the critical Taylor number, the aspect ratio Γ of the flow, and the particle concentration in Taylor-Dean flow. Adnane *et al*. [17] examined experimentally the effect of inclination angle on different flow regimes occurring in a partially filled space between two coaxial cylinders. They found that varying filling ratios and tilt angles of Taylor-Couette flow system significantly affect the flow profiles. Numerical investigation explores hydrodynamic stability in viscous flow between a periodically varying inner cylinder and a fixed outer cylinder using Fluent software was analyzed by Oualli *et al*. [18]. Simulations highlight early flow transition under radial pulsatile motion on the inner cylinder, revealing a significant decrease in the critical Taylor number, signaling early turbulence onset. This finding has practical implications for enhancing transport phenomena in industrial applications such as reactors and heat exchangers.

Recently, Dandelia *et al*. [19] interested in the optimal control of instability growth in Taylor-Couette flow. Their results indicate a reduction in the growth rate and the typical energy perturbation growth by about 72%.

The present study aims to numerically investigate how the shape of end walls affects the formation of Ekman cells and Taylor vortices. Four geometries are considered: (A) plate endwalls, (B) hemispherical upper endwall and lower plate endwall, (C) upper plate endwall and hemispherical lower endwall, and (D) hemispherical upper and lower endwalls. Additionally, the study analyzes the skin friction coefficient near the onset of Ekman cells and Taylor vortices.

2. Mathematical formulation

2.1. Physical model

Figure 1 depicts the four geometries studied: (A) plate endwall, (B) hemispherical upper-endwall, (C) hemispherical upper-endwall and hemispherical lower, and (D) hemispherical lower and upper-endwall. The working fluid, an aqueous solution, has a dynamic viscosity of $\mu = 48\ mPa{\cdot}s$ and a density of $\rho = 1050\ kg/m^3$ at a temperature of $T = 22°C$. The radius ratio is $\eta = 0.9$, and the aspect ratio is $\Gamma = 9.85$.
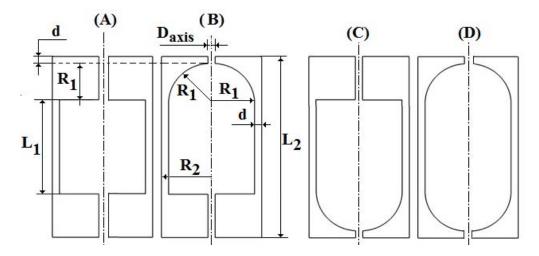

Fig.1. Different geometries of the studied flow system.

2.2. Governing equations

The governing equations of the flow are the continuity and the momentum equations which are presented as follow,
- Continuity equation

$$\frac{1}{r}\frac{\partial(ru_r)}{\partial r} + \frac{\partial u_z}{\partial z} = 0 , \tag{2.1}$$

- Momentum equations

$$\frac{\partial u_r}{\partial t} + u_r\frac{\partial u_r}{\partial r} + u_z\frac{\partial u_r}{\partial z} + \frac{u_\theta^2}{r} = -\frac{\partial p}{\partial r} + \frac{1}{\text{Re}}\left[\Delta u_r - \frac{u_r}{r^2}\right],$$

$$\frac{\partial u_z}{\partial t} + u_r\frac{\partial u_z}{\partial r} + u_z\frac{\partial u_z}{\partial z} = -\frac{\partial p}{\partial z} + \frac{1}{\text{Re}}\left[\Delta u_z\right], \tag{2.2}$$

with

$$\Delta = \frac{\partial^2}{\partial r^2} + \frac{1}{r}\frac{\partial}{\partial r} + \frac{\partial^2}{\partial z^2}$$

and Re is Reynolds number given by,

$$\text{Re} = \frac{\rho\Omega_1 R_1 d}{\mu} . \tag{2.3}$$

Taylor number is defined as,

$$Ta = \text{Re}\sqrt{\frac{d}{R_1}} \tag{2.4}$$

- Boundary conditions

- $0 < z < H$ and $r = R_1$, $V_1 = \Omega_1 R_1$ and $\Omega_1 > 0$,

- $0 < z < H$ and $r = R_2$, $V_2 = \Omega_2 R_2$ and $\Omega_2 = 0$,

  $\tag{2.5}$

- $z = 0$ and $R_1 < r < R_2$, $V_2 = \Omega_2 R_2$ and $\Omega_2 = 0$,

- $z = H$ and $R_1 < r < R_2$, $V_2 = 0$, $V_2 = \Omega_2 R_2$ and $\Omega_2 = 0$.

3. Computational method

The flow between two coaxial cylinders was simulated using the CFD software Ansys Fluent 14.0, employing the finite volume method [20]. The momentum equation was solved using the SIMPLE method, and the pressure correction equation was interpolated using the third-order QUICK scheme with body force weighted.

The physical model and meshes were created using GAMBIT 2.3.16. Due to the axisymmetric nature of flow between concentric rotating cylinders, the geometry was modeled in two dimensions. Several tests were conducted to determine the optimal grid resolution, as illustrated in Fig.2. A structured grid consisting of *28* cells in the radial direction and *224* cells in the axial direction was selected.
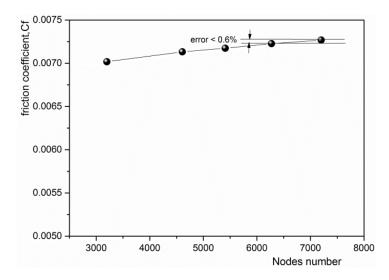

Fig.2. Evolution of the critical Taylor number versus grid cells number.

3.1. Validation model

The numerical model employed in this study was validated against experimental data provided by Sobolik *et al*. [10]. Their study measured the azimuthal velocity gradient distribution at a fixed cylindrical wall. Our results exhibit good agreement with those reported by Sobolik *et al*. [10], as depicted in Fig.3.
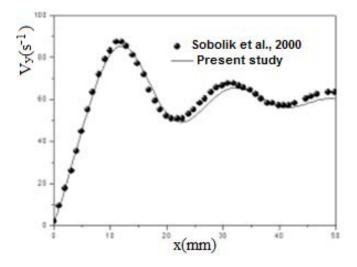

Fig.3. Distribution of azimuthal velocity gradient near the fixed cylindrical wall.

4. Results and discussion

In the Taylor-Couette flow system, where the inner cylinder rotates within a fixed outer cylinder, various flow regimes emerge. The structure of the flow is significantly influenced by the characteristics of the endwalls. At very low Taylor numbers, small cells are observed near the upper and lower endwalls.

4.1. Effect of endwall shapes on the streamline contours development

For configuration (A), two Ekman cells appear on the upper and lower plate endwalls (see Fig.4 (A)). In configurations (B-D) with hemispherical endwalls, two partly hemispherical vortices are observed, with a smaller cell near the Ekman cells and a larger cell at the equator (see Fig.4 (B-D)). In these cases, the appearance of Ekman cells is delayed by approximately *44%* compared to the base case in Fig.4 (A), as the Taylor number increases from $Ta = 30$ to $Tac = 43.5$ (see Fig.4 (A-D)). Beyond this threshold, Taylor vortices develop, characterized by a secondary periodic axial wave movement along the stationary axial direction of the basic flow. It is evident that changing the endwall shape from a plate to a hemispherical form significantly influences flow structures, resulting notable variation in Ekman cell configurations.
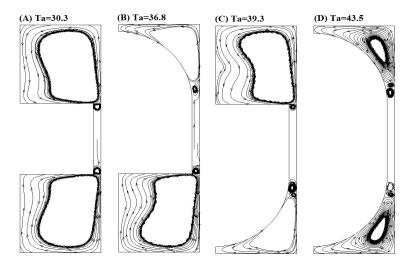

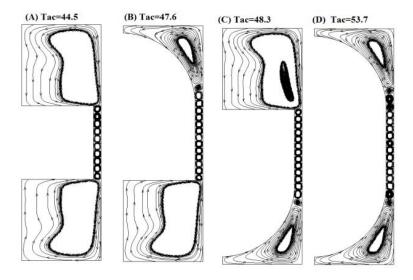Fig.4. (A-D). Development of stream function contours at the onset of Ekman cells.

Fig.5. (A-D). Development of stream function contours at the onset of Taylor vortices.

From Fig.5 (A-D), we observe a transition from spherical Couette flow to Taylor-vortex flow in the hemisphere. This transition is accompanied by a pinch (o-vortex flow) adjacent to the Ekman cells, and a large vortex occupies the annular space of the hemisphere part. Furthermore, the circulation in the closed pinch streamlines always has the same sign as that in the large basic vortex, because it is not separated from

the large basic vortex by an inlet or outlet boundary. When the Taylor number exceeds Tac $(Ta > Tac)$, the base vortex in the flow develops a pinch. Changes in the shape of the endwalls, from flat plate endwalls to hemispherical endwalls, are observed to have a significant effect on the flow structures, causing substantial changes in the shape of vortices. Therefore, as the endwall shape changes from flat plate to hemispherical, the circular shape of Taylor vortices near the endwall changes to elliptical form.

4.2. The effect of endwall shapes on the contours development of axial velocity

Figure 6 (A-D) displays the evolution of axial velocity contours versus Taylor number for different configurations. Starting from a low Taylor number and the appearance of Ekman cells, we observe the development of axial velocity contours near the endwalls. In configurations with upper or lower hemispherical endwalls and at the equator, we observe the development of two cells: a small one close to the Ekman cell and a large cell (see Fig.6 (B-D)).
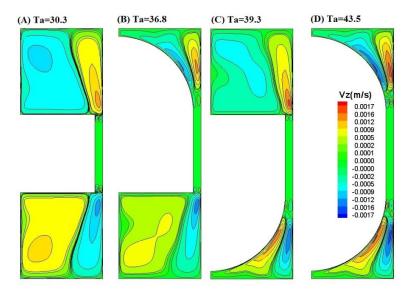

Fig.6.(A-D). Development of axial velocity contours at the onset of Ekman cells.
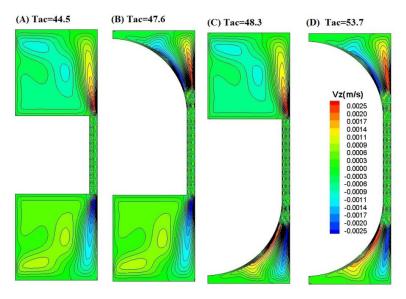

Fig.7.(A-D). Development of axial velocity contours at the onset of Taylor vortices.

As we increase the Taylor number from *Ta = 30* up to *Tac = 44* , as shown in Fig.6(A), changing the shape of the endwall from a flat plate to a hemispherical endwall strongly affects the flow structures, causing substantial changes in the shape of Ekman cells near the endwall. Continuing to increase the Taylor number leads to the appearance of Taylor vortices occupying the entire annular space, characterized by the onset of the first instability.

From Fig.7 (A-D), we observe the development of two cells in the annular space of the hemisphere. One large cell circulates counterclockwise around the main vortex in the upper hemisphere, and the other cell is adjacent to the top of the cylindrical part. Based on these results, we conclude that varying the endwall shape from a flat plate to a hemispherical significantly affects the shape of the vortices.

4.3. Effect of endwall shapes on the evolution of skin friction coefficient

In the following section, we present and analyze the variation of the skin friction coefficient on the wall of the external cylinder as Ekman cells and Taylor vortices begin to appear. The formula used to calculate the coefficient of friction is given by Eq.(4.1).
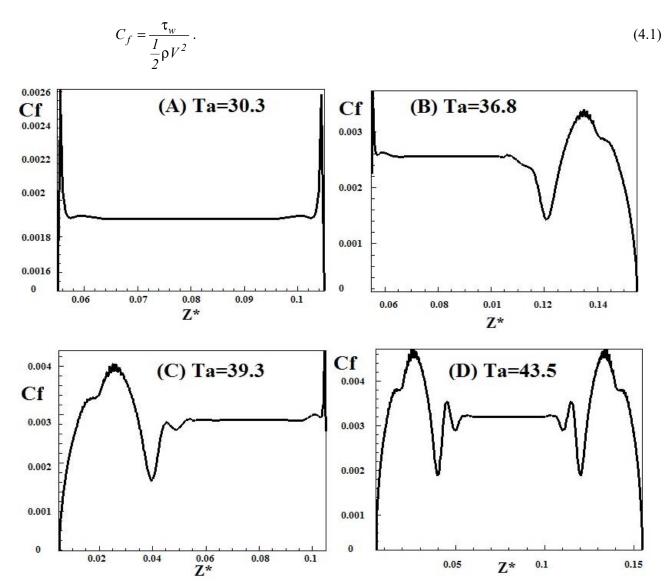
$$C_f = \frac{\tau_w}{\frac{1}{2}\rho V^2} . \qquad (4.1)$$

Fig.8.(A-D). Evolution of the skin friction coefficient upon the appearance of Ekman cells.

Figure 8(A-D) illustrates the evolution of the skin friction coefficient on the external cylinder wall during the formation of Ekman cells.

From Fig.8 (A-D), the skin friction coefficient values are significantly higher near the outer cylinder wall. We observe a reduction of approximately *21%* in the skin friction coefficient for the hemispherical upper endwall configuration compared to the nominal case (see Fig.8(B)). In the case of both upper and lower hemispherical configurations, at the onset of Ekman cells, the skin friction decreases by about *43%* as shown in Fig.8(D).

Fig.9 (A-D) illustrates the development of the skin friction coefficient on the outer cylinder wall at the onset of vortices. It shows a reduction of the skin friction coefficient by around *20%* compared to the nominal case near the transition from Couette flow to Taylor vortices.
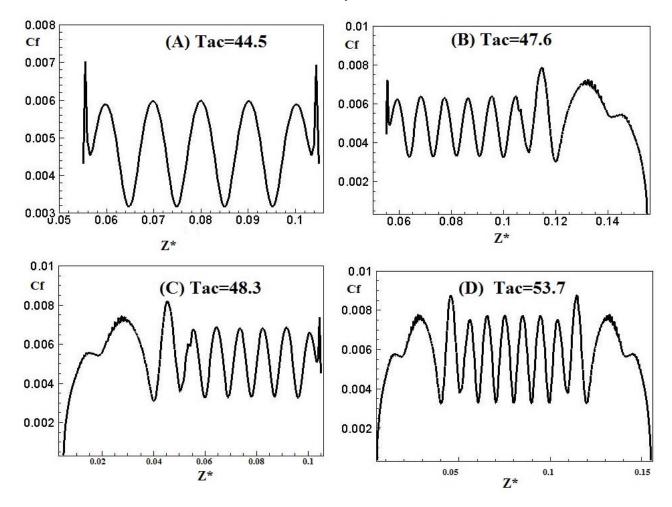

Fig.9(A-D). Evolution of the skin friction coefficient at the onset of Taylor vortices.

5. Conclusions

This numerical investigation focuses on the effect of the endwall shape on fluid flow confined between two concentric cylinders. The study aims to enhance the stability of Taylor-Couette flow by modifying the endwall shape from a flat plate to a hemispherical configuration. We specifically investigate the critical thresholds for the onset of Ekman cells and Taylor vortices. The evolution of the Taylor number for various configurations and its impact on flow behavior within the annular space between the cylinders are simulated and discussed.

The results indicate that changes in the endwall shape strongly influence the shape of axial velocity contours near the endwall. Specifically, for configurations with lower and upper hemisphere endwalls,

stability is improved by approximately *20%* compared to the nominal case. The modification from a flat plate to a hemispherical endwall significantly affects flow structures, leading to substantial changes in the shapes of Ekman cells and Taylor vortices.

For the upper and lower hemispherical configurations, the skin friction coefficient is reduced by approximately *43%* at the onset of Ekman cells and by about *20%* at the appearance of Taylor vortices compared to the nominal case with a flat plate endwall.

Acknowledgements

Nomenclature

C_f – skin friction coefficient

d – annular space

g – acceleration due to gravity

H – cylinders length

r, θ, z – radial, azimuthal, axial coordinate

R_1 – inner cylinder radius

R_2 – outer cylinder radius

T – temperature

Ta – Taylor number

Tac – critical Taylor number

u_r, u_θ, u_z – radial, azimuthal and axial velocity component

V_y – gradient of azimuthal velocity at the outer wall

V_1 – inner cylinder velocity

V_2 – outer cylinder velocity

Γ – aspect ratio

δ – gap ratio

η – radius ratio

μ – dynamic viscosity

ν – kinematic viscosity

ρ – fluid density

τ – shear stress

Ω_1 – inner rotational velocity

Ω_2 – outer rotational velocity

Ω_3 – endwall rotational velocity

References

[1] Lee Y.B., Kwak H.D., Kim C.H., and Lee N.S. (2005): *Numerical prediction of slip flow effect on gas-lubricated journal bearings for MEMS/MST-based micro-rotating machinery.*– Tribology International vol.38, No.2, pp.89-96.

[2] Bouabdallah A. and Cognet G. (1980): *Laminar-turbulent transition in Taylor-Couette flow.*– in Laminar Turbulent Transition, (IUTAM Conference), edited by R. Eppler and H. Fasel (Springer-Verlag, Berlin), pp.368-377.

[3] Pfister G. and Rehberg I. (1981): *Space-dependent order parameter in circular Couette flow transitions.*– Physics Letters A, vol.83, No.1, pp.19-22.

[4] Cliffe K.A. and Mullin T. (1985): *A numerical and experimental study of anomalous modes in the Taylor experiment.*– Journal of Fluid Mechanics, vol.153, pp.243-258.

[5] Taylor G.I. (1923): *Stability of a viscous liquid contained between two rotating cylinders.*– Philosophical Transactions of the Royal Society of London, Series A, Containing Papers of a Mathematical or Physical.

[6] Abshagen J., Heise M., Langenberg J. and Pfister G. (2007): *Imperfect Hopf bifurcation in spiral Poiseuille flow.*– Physical Review E, vol.75, No.1, p.016309.

[7] Hoffmann C., Lücke M. and Pinter A. (2005): *Spiral vortices traveling between two rotating defects in the Taylor-Couette system.*– Physical Review E, vol.72, No.5, p.056311.

[8] Snyder H.A. (1968): *Stability of rotating Couette flow. I. Asymmetric waveforms.*– Physics of Fluids, vol.11, No.4, pp.728-734.

[9] Heise M., Hochstrate K., Abshagen J. and Pfister G. (2009): *Spirals vortices in Taylor-Couette flow with rotating endwalls.*– Physical Review E, vol.80, No.4, p.045301.

[10] Sobolik V., Izrar B., Lusseyran F. and Skali S. (2000): *Interaction between the Ekman layer and the Couette-Taylor instability.*– International Journal of Heat and Mass Transfer, vol.43, No.24, pp.4381-4393.

[11] Sobolik V., Jirout T., Havlica J. and Kristiawan M. (2011): *Wall shear rates in Taylor vortex flow.* – Journal of Applied Fluid Mechanics, vol.4, pp.25-31.

[12] Czarny O., Serre E., Bontoux P. and Lueptow R.M. (2003): *Interaction between Ekman pumping and the centrifugal instability in Taylor-Couette flow.* – Physics of Fluids, vol.15, No.2, pp.467-477.

[13] Avila M., Grimes M., Lopez J. M. and Marques F. (2008): *Global endwall effects on centrifugally stable flows.*– Physics of Fluids, vol.20, No.10, p.104104.

[14] Poncet S., Da Soghe R., Bianchini C., Viazzo S. and Aubert A. (2013): *Turbulent Couette-Taylor flows with endwall effects: A numerical benchmark.*– International Journal of Heat and Fluid Flow, vol.44, pp.229-238.

[15] Daimallah A., Bouabdallah A., Nsom B., Adnane M. and Alemany A. (2009): *Onset of instabilities in Taylor-Dean flow of yield-stress fluid.*– Applied Rheology, vol.19, No.3, p.33960.

[16] Daimallah A. (2013): *Etude des phénomènes d'instabilités en présence d'une suspension dans l'écoulement de Taylor-Dean.*– Thèse de Doctorat en Cotutelle entre USTHB-Alger, Algérie et UBO-Brest, France.

[17] Adnane E., Lalaoua A. and Bouabdallah A. (2016): *An experimental study of the laminar-turbulent transition in a tilted Taylor-Couette system subject to free surface effect.*– Journal of Applied Fluid Mechanics, vol.9, No.3, pp.1097-1104, doi:10.18869/acadpub.jafm.68.228.24743.

[18] Oualli H., Mekadem M., Lebbi M. and Bouabdallah A. (2015): *Taylor-Couette flow control by amplitude variation of the inner cylinder cross-section oscillation.*– The European Physical Journal Applied Physics, vol.71, No.1, p.11102.

[19] Dandelia H., Kant R. and Narayanan V. (2022): *Optimal control of growth of instabilities in Taylor-Couette flow.*– Physics of Fluids, vol.34, p.044106, https://doi.org/10.1063/5.0086971.

[20] Eymard R., Gallouët T. and Herbin R. (2000): *Finite volume methods.*– Handbook of Numerical analysis, vol.7, pp.713-1018, https://doi.org/10.1016/S1570-8659(00)07005-8.